CrossMark

Mechanical Properties and Microstructure of TIG and FSW Joints of a New Al-Mg-Mn-Sc-Zr Alloy

Guofu Xu, Jian Qian, Dan Xiao, Ying Deng, Liying Lu, and Zhimin Yin

A new Al-5.8%Mg-0.4%Mn-0.25%Sc-0.10%Zr (wt.%) alloy was successfully welded by tungsten inert gas (TIG) and friction stir welding (FSW) techniques, respectively. The mechanical properties and microstructure of the welded joints were investigated by microhardness measurements, tensile tests, and microscopy methods. The results show that the ultimate tensile strength, yield strength, and elongation to failure are 358, 234 MPa, and 27.6% for TIG welded joint, and 376, 245 MPa and 31.9% for FSW joint, respectively, showing high strength and superior ductility. The TIG welded joint fails in the heat-affected zone and the fracture of FSW joint is located in stirred zone. Al-Mg-Mn-Sc-Zr alloy is characterized by lots of dislocation tangles and secondary coherent $Al_3(Sc,Zr)$ particles. The superior mechanical properties of the TIG and FSW joints are mainly derived from the Orowan strengthening and grain boundary strengthening caused by secondary coherent $Al_3(Sc,Zr)$ nano-particles (20-40 nm). For new Al-Mg-Mn-Sc-Zr alloy, the positive effect from secondary $Al_3(Sc, Zr)$ particles in the base metal can be better preserved in FSW joint than in TIG welded joint.

1. Introduction

Non-age-hardenable Al-Mg-Mn alloy is widely used in the field of aerospace industry due to its high strength, good weldability, and admirable corrosion resistance (Ref 1, 2). Of all micro-alloying additions to Al, Sc and Zr offer the greatest potential for developing new lightweight structural materials with excellent mechanical property and desirable corrosion resistance, due to the formation of extremely fine, coherent $Al_3(Sc, Zr)$ particles with $L1_2$ structure, which can effectively refine grains and inhibit recrystallization (Ref 3-5). Compared with the traditional medium-strength weldable Al-Mg alloy, the new Al-Mg-Mn-Sc-Zr alloy exhibits more excellent mechanical property. It belongs to a new generation lightweight structural material (Ref 6-9).

The welding of aluminum alloys has received renewed attention, because of the need to reduce the high manufacturing costs associated with the fabrication of riveted, or fastened structures. Tungsten inert gas (TIG) welding process is the most widely used welding technology for aluminum alloys (Ref 10). However, some problems should be noted on this technology, such as porosity, hot-cracking, and as-cast coarse microstructure (Ref 11). These welding defects can deteriorate the

mechanical properties of the joints. Friction stir welding (FSW), developed by The Welding Institute (TWI) in 1991, is a new solid-state joining technology. During FSW process, a non-consumable rotating tool with a special designed pin and a shoulder is plunged into the gap of the work-pieces being welded to a preset depth and moved along the weld joint. Heat is generated through the frictional contact between the rotating tool shoulder and abutting material surface and plastic deformation of work-piece (Ref 12-14). It is energy efficient, environment friendly, and versatile. Because of the low heat input, material subjected to FSW does not melt and recast, and thus the solidification defects, such as dendritic segregation and porosity, which are usually formed in fusion welding process, can be avoided (Ref 15, 16). Although there are some reports about the microstructure and mechanical property of Al-Mg-Mn welded joints, with the development of aerospace technology, it still needs to further improve the strength and ductility of the welded structure (Ref 11, 17). Moreover, the limited understanding on the relationship between the microstructure and mechanical property significantly limits the application of the new Al-Mg-Mn-Sc-Zr alloy.

In this paper, we try to weld a new Al-Mg-Mn-Sc-Zr alloy plate by TIG and FSW techniques, and to establish the relationship between microstructure and mechanical property of the new welded joints. The results are of great importance to provide theoretical and experimental basis for further developing superior light-weight welded structure.

2. Experimental Methods

2.1 Materials and Welding

2 mm annealed Al-5.8%Mg-0.4%Mn-0.25%Sc-0.1%Zr alloy (wt.%) plates were welded by TIG and FSW processes, respectively. The welded plates were then annealed at 300 °C for 1 h.

TIG welding was conducted along the rolling direction of plate at China Aerospace Research Institute of Materials &

Jian Qian, Dan Xiao, and **Zhimin Yin**, School of Materials Science and Engineering, Central South University, Hunan, Changsha 410083, China; **Guofu Xu** and **Ying Deng**, School of Materials Science and Engineering, Central South University, Hunan, Changsha 410083, China and State Key Laboratory of Powder Metallurgy, Central South University, Changsha 410083, China; **Liying Lu**, Northeast Light Alloy Co. Ltd, Hei Longjiang, Harbin 150060, China. Contact e-mail: csudengying@163.com.

Processing Technology. The welding wire for TIG welding was Al-6.5Mg-0.25Sc-0.15Zr-0.1Cr-0.02Ti-0.003B alloy (wt.%) with a diameter of 3 mm; the flow rate of argon shield was 14 L/min; the welding voltage and current were 14 V and 250 A, respectively, and the speed of welding was 6 mm/s.

FSW was conducted parallel to the rolling direction in Beijing FSW Technology Co. Ltd. Friction stir tool was composed of a truncated cone-shaped pin with a diameter of 2 mm and a shoulder with a diameter of 10 mm. The tool rotation speed and the travel speed of the tool were 600 rpm and 200 mm/min, respectively.

2.2 Mechanical and Microhardness Tests

The mechanical properties of all studied weld joints were evaluated by room temperature tensile tests, which were carried out at a strain rate of 1×10^{-6} s^{-1}, using transverse oriented tensile specimens (the long axis of tensile specimens was perpendicular to the welding direction or the rolling direction) with a gauge length of 70 mm and a width of 12 mm, designed according to the specification in IS0 4136 (2001): Destructive tests on welds in metallic materials. A minimum of three mechanical tests were performed on each sample, and their average values are reported in this study.

Vickers microhardness testes were performed on the polished surface of the weld joint. The hardness data were obtained at a distance interval of 1 mm by applying a load of 200 g for 10 s.

2.3 Microstructure Observations

For optical microscopy observations, the weld joints were ground, polished and anodized using fluorboric acid (4 ml 40%HBF$_4$ + 100 ml distilled water) under voltage of 16 V for 120s, and then examined on a Leica EC3 optical microscope.

Thin foils for transmission electron microscope (TEM) observation were mechanically grounded to the thickness of about 80 μm, and then electro-polished by double-jet electro-polishing in a solution consisting of 30% nitric acid and 70% methanol solution at 20 V and −30 °C, and finally observed on a Tecnai G^{2}20 electron microscope, with an acceleration voltage of 200 kV.

The fracture surface was observed on Sirion 200 field emission gun scanning electron microscope equipped with energy dispersive x-ray spectroscopy system.

3. Results

3.1 Microhardness

The microhardness distributions across the transverse cross section of the TIG and FSW joints are shown in Fig. 1. TIG weld joint is composed of fusion zone (FZ) and heat-affected zone (HAZ). FSW joint consists of stirred zone (SZ), thermo-mechanically affected zone (TMAZ), and HAZ. With the increase of the distance away from the weld center to the base metal, the hardness decreases slightly and then gradually increases to the level of base metal in two kinds of welded joints. The lowest microhardness values are located at the transition zone between the SZ and TMAZ in FSW joint and at the transition zone between the FZ and HAZ in TIG welded
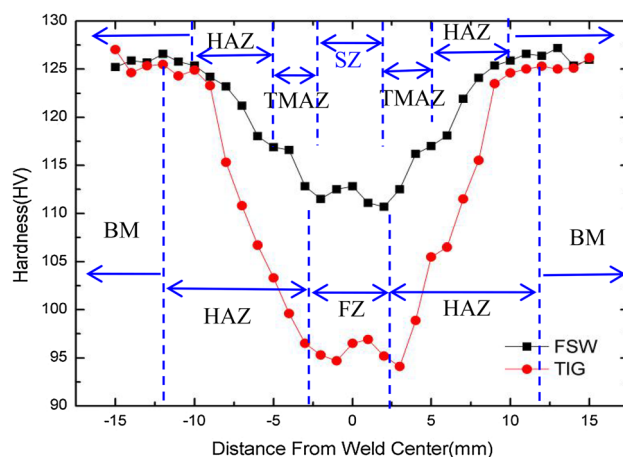

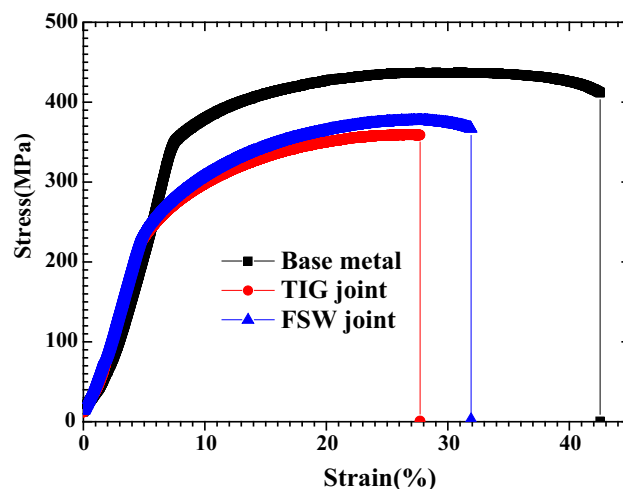**Fig. 1** Microhardness distributions of TIG and FSW joints

Fig. 2 Strain-stress curves of base metal, and TIG and FSW joints

joint. Compared with the TIG welded joint, FSW joint shows higher hardness in the welded zone.

3.2 Mechanical Property

Stress-strain curves of base metal and TIG and FSW joints are shown in Fig. 2. It can be found that the stress increases rapidly and then holds constant or decreases to some extent after attaining a peak value with the increase of strains. Table 1 lists the ultimate tensile strength (UTS), yield strength (YS), elongation to failure (E_f), and welding coefficient. It can be found that, compared with the mechanical property of base metal, there is a great loss in mechanical property in two welded joints. However, the TIG and FSW joints of the new alloy exhibit higher strength and admirable ductility. For TIG welded joint, the UTS, YS, elongation to failure are 358, 234 MPa, and 27.6%, respectively, and for FSW joint, the corresponding values are 376, 245 MPa, and 31.9%, respectively. The mechanical property values of the studied TIG and FSW joints are much superior to the corresponding welded joints of the reported Al-Mg and Al-Mg-Sc alloy (Ref 17-19).
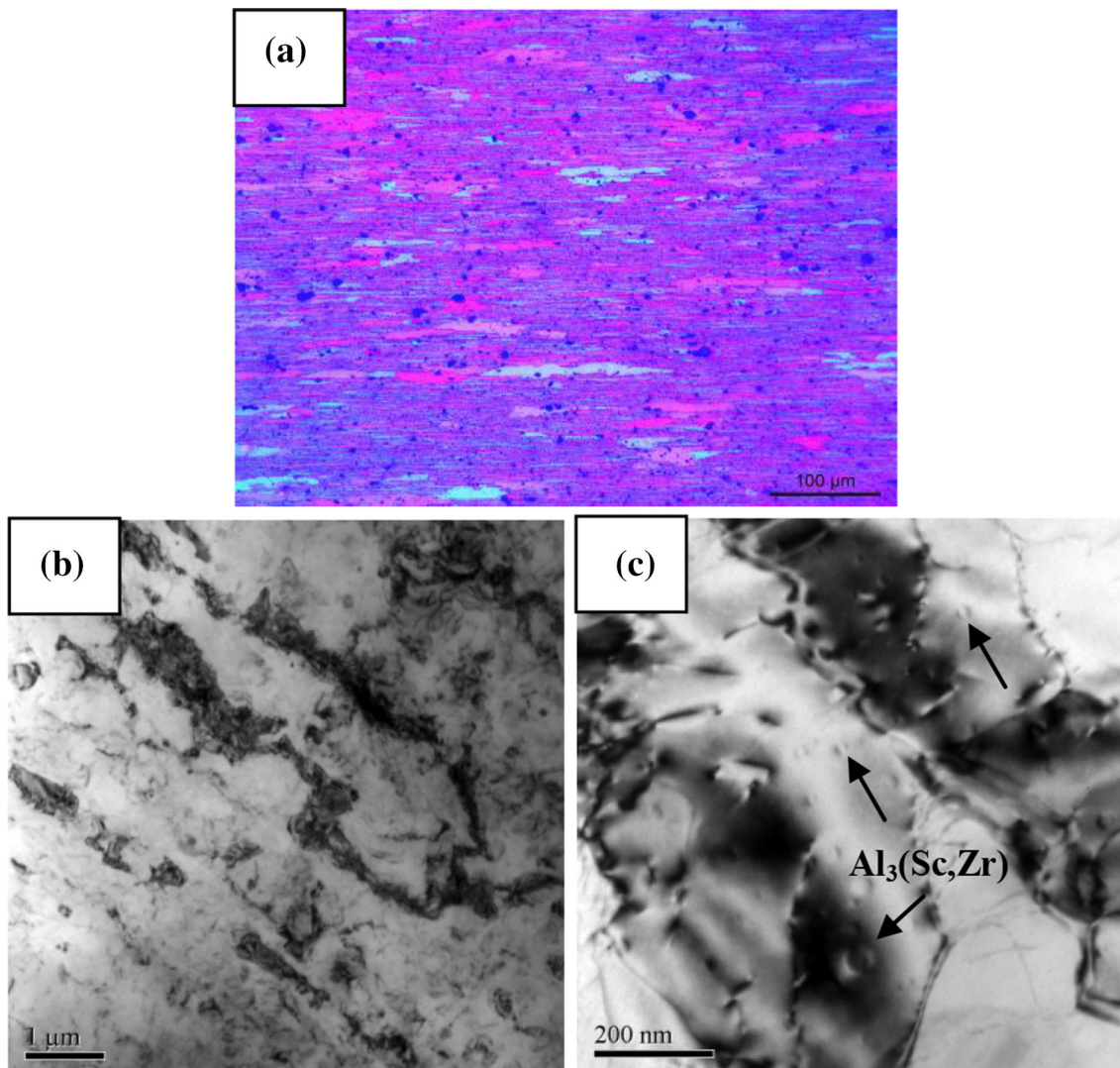
3.3 Microstructure

3.3.1 Base Metal. Figure 3 shows the microstructure of Al-Mg-Mn-Sc-Zr alloy. It can be found that the alloy is characterized by elongated fiber-like non-recrystallized structure along the rolling direction (Fig. 3a). TEM bright field image indicates that lots of dislocation tangles or recovery structures exist in the interior of the deformed grains (Fig. 3b). By magnified observation, a large number of secondary coherent $Al_3(Sc,Zr)$ particles in the size of about 20-40 nm, judged by their Ashby-Brown contrast for bright-field TEM images, are distributed in the grains (Fig. 3b). $Al_3(Sc,Zr)$

Table 1 Mechanical property of base metal, and TIG and FSW joints

Condition	UTS, MPa	YS, MPa	EI, %	Welding coefficient, %
BM	433	341	42.5	⋯
TIG welded joint	358	234	27.6	0.83
FSW joint	376	245	31.9	0.87

particles can strongly pin dislocation and sub-grain or grain boundaries and inhibit the occurrence of recrystallization during the thermal-mechanical process of the preparation of plates (Ref 2, 6, 7, 12, 20). This is why the new Al-Mg-Mn-Sc-Zr alloy still remains non-recrystallized structure.

3.3.2 TIG Welded Joint. Figure 4 shows the optical and TEM microstructure of the TIG welded joint. Macrostructure of the transverse cross section of TIG joint (Fig. 4a) indicates that there are no macro-level cracks, revealing that the welding wire has a good compatibility with the matrix. Besides, it can be found that, from the weld center to the base metal, the thickness of the welded joint gradually decreases until it reaches to the level of base metal. Based on the microstructural characterization, two zones, i.e., FZ and HAZ, can be identified in the joint. The FZ, as shown in Fig. 4(b), exhibits a typical dendritic structure, and a small number of gas cavities with various magnitudes can be observed. The HAZ is characterized by coarsened elongated grains due to the heat input during the welding process (Fig. 4c). Based on the TEM results, it can be concluded that nano-scaled $Al_3(Sc,Zr)$ particles have dissolved into the matrix completely in FZ (Fig. 4d), while they remain the nano-scaled size in the HAZ (Fig. 4e). Those particles can


Fig. 3 Microstructure of Al-Mg-Mn-Sc-Zr alloy (a) optical image, (b) and (c) TEM bright field images
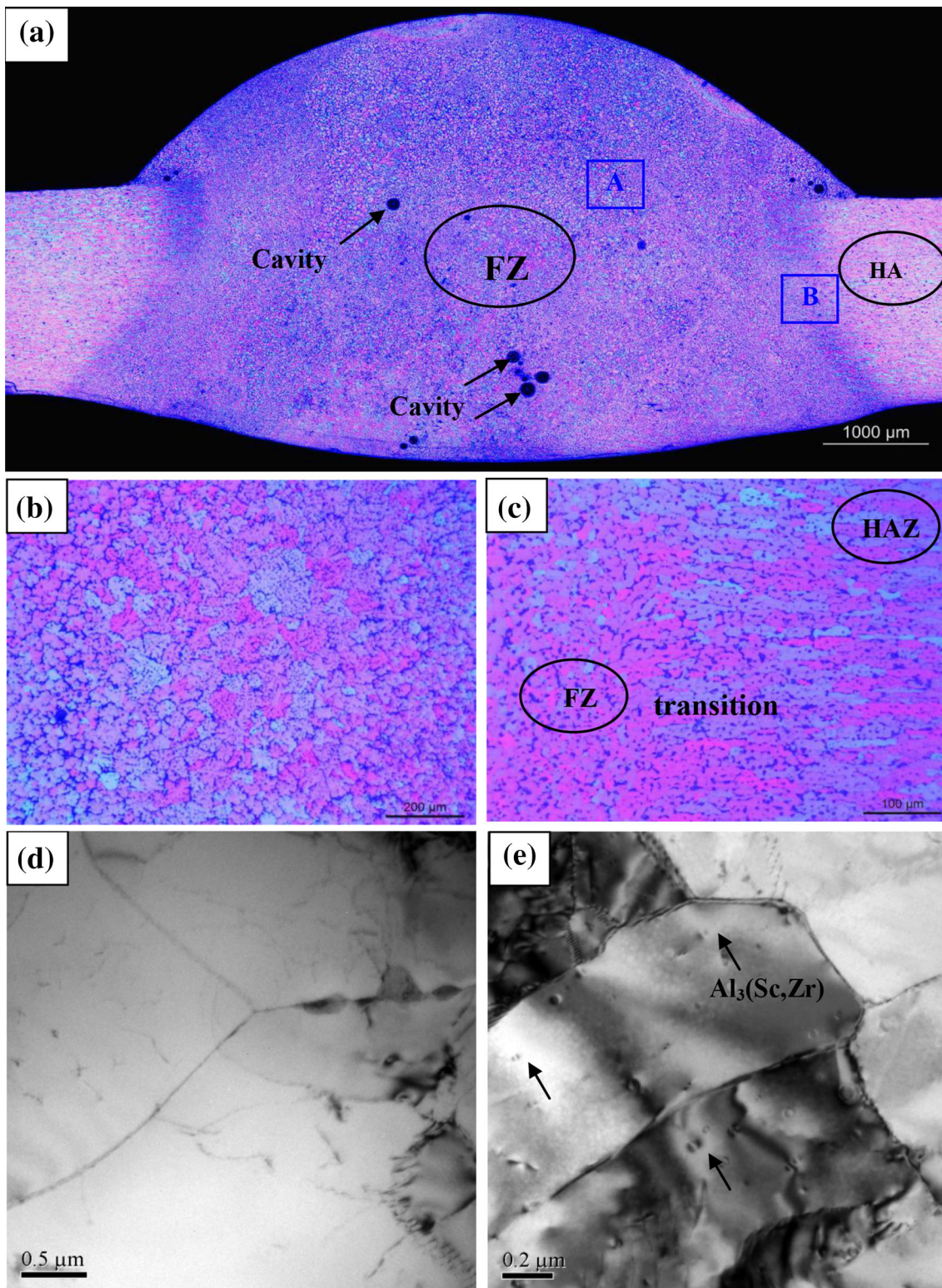
Fig. 4 Microstructure of TIG welded joint, OM: (a) macrostructure, (b) fusion zone (magnified image of zone A in (a)), (c) heat-affected zone (magnified image of zone B in (a)), TEM bright field image (d) fusion zone, (e) heat-affected zone

strongly pin dislocation and grain or subgrain boundaries to restrain the occurrence of recrystallization and the growth of grains during welding process. This is why the HAZ still remains un-recrystallized sub-grain structure.

3.3.3 FSW Joint. Figure 5 shows the optical and TEM microstructure of the FSW joint. According to the macro-graph (Fig. 5a), it can be found that the weld center is the thinnest zone in the whole welded joint. Moreover, with the increase of
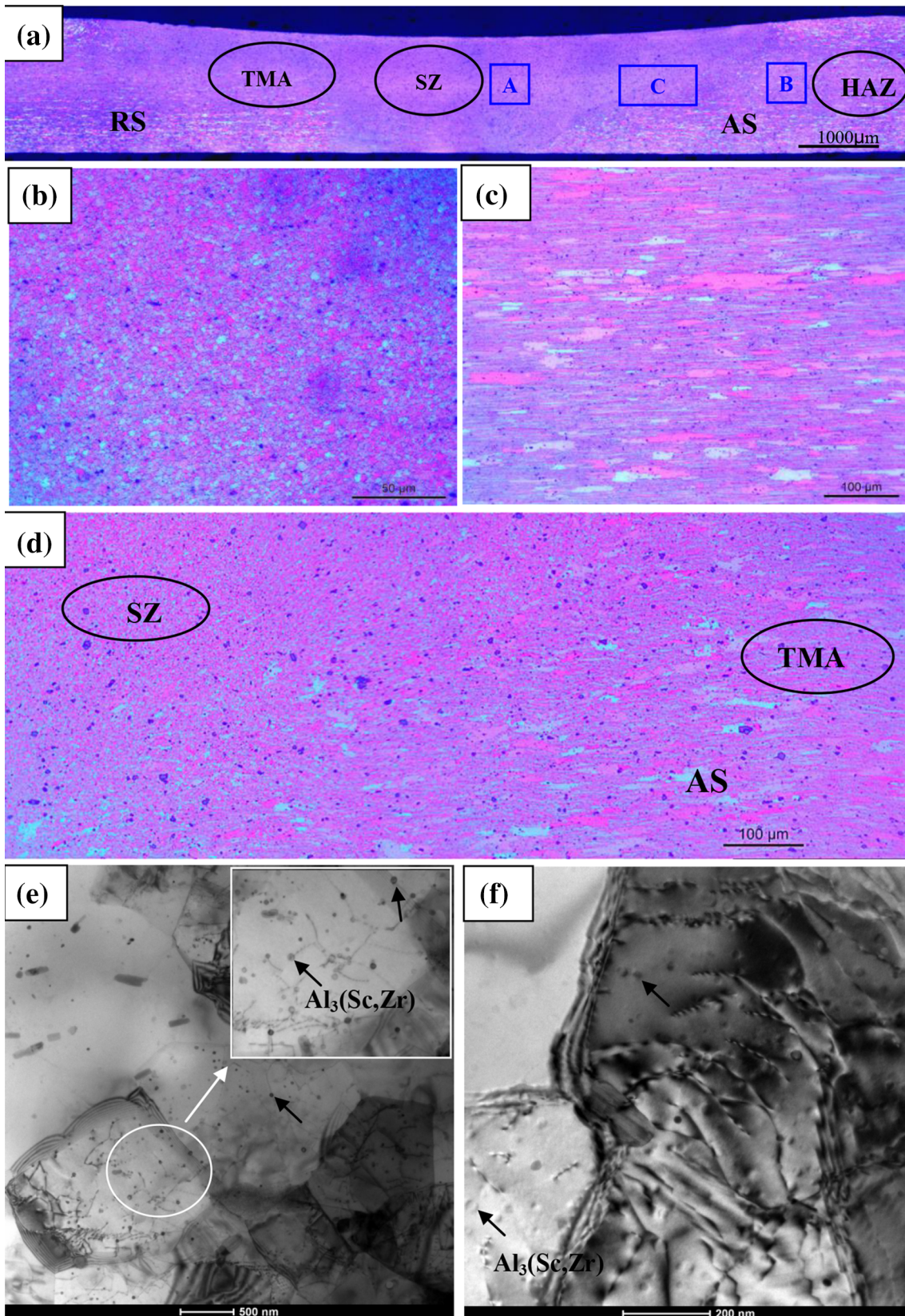
Fig. 5 Microstructure of FSW joint, OM: (a) macrostructure; (b) stirred zone (magnified image of zone A in (a)); (c) heat-affected zone (magnified image of zone B in (a)), (d) transition zone between stirred zone and thermo-mechanical-affected zone on the advancing side (magnified image of zone C in (a)), TEM: (e) stirred zone, (f) heat-affected zone
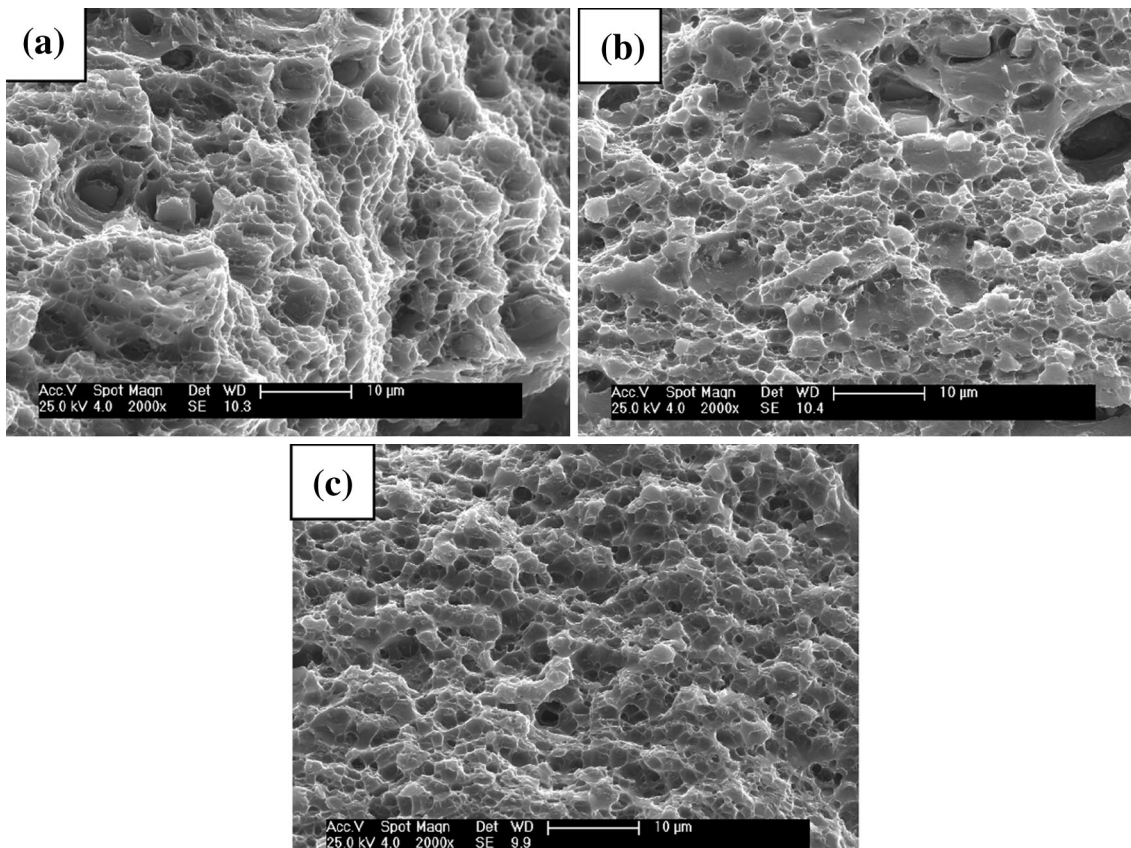
Fig. 6 Fracture surface (a) BM, (b) TIG joint, (c) FSW joint

the distance away from the weld center to the base metal, the thickness gradually increases until it reaches the level of base metal.

The FSW joint can be divided into three distinct microstructural zones, i.e., SZ, TMAZ, and HAZ. The retreating side and advancing side are denoted as RS and AS in Fig. 5(a). Intense plastic deformation and frictional heating during FSW result in generation of fine-grained microstructures in SZ (Fig. 5b). HAZ is composed of fibrous grains (Fig. 5c). Compared with the base metal, it can be found that there is no apparent grain growth in HAZ. Due to the experience of severely plastic deformation, the TMAZ is characterized by a highly deformed structure (Fig. 5d). According to the TEM results, there are many dispersed $Al_3(Sc,Zr)$ particles in SZ and HAZ. $Al_3(Sc,Zr)$ particles preserved owe to its good thermal stability and the relatively low heat input during FSW process (Fig. 5e and f). These $Al_3(Sc,Zr)$ particles can strongly pin the movement of dislocations and the immigration of grain or subgrain boundaries, as arrowed in Fig. 5(e) and (f), leading to refined grains and a higher fraction of small angle gain boundaries associated with substructure.

3.3.4 Fracture Surface. Visual examination on the fractured TIG welded joint, it can be found that the joint fails in HAZ. According to the hardness distribution in Fig. 1, FZ is the weakest zone in the whole TIG welded joint; thus fracture is supposed to occur in this zone. However, the excess weld metal (as shown in Fig. 4a) provides extra strength at this zone. TIG welded joint finally failed at the HAZ. For FSW joint, fracture occurs in the weld center, due to its thinnest thickness and relatively low strength.

Figure 6 shows fracture morphology of base metal and TIG and FSW joints. BM and TIG and FSW joints all fracture in ductile transgranular fracture mode. There are lots of dimples, indicating a good ductility for the studied alloy and welded joints. By comparison, the dimples of TIG welded joint are relatively shallow and some flat regions can be found, revealing a relative poor ductility.

4. Discussion

4.1 Relationship Between Microstructure and Mechanical Properties of TIG and FSW Joints

The base metal has a deformed fibrous subgrains structure with lots of dislocations and dispersively distributed nano-scaled $Al_3(Sc,Zr)$ particles. The main strengthening mechanism of the studied Al-Mg-Mn-Sc-Zr alloy includes solution strengthening, substructure strengthening, precipitation strengthening derived from $Al_3(Sc,Zr)$ particles and grain boundary strengthening (Ref 19). Precipitation strengthening of particles can generally occur by one of two mechanisms, depending on the particle size. These are (i) shearing of small precipitates; and (ii) the Orowan bypass mechanism for larger particles. With an increase in particle diameter, the strength increases when the first mechanism operates, while it decreases when the Orowan mechanism operates. Transition from the shearing mechanism to the Orowan strengthening mechanism occurs in the particle diameter range from 4 to 6 nm (Ref 7),

suggesting that the Orowan mechanism should be responsible for the $Al_3(Sc, Zr)$ particle-induced precipitation strengthening in our studies (20-40 nm).

During the welding process, the weld heat can lead to the coarsening or growth of grains, the merging of subgrains, and the movement of dislocations (Ref 21). As the $Al_3(Sc, Zr)$ are coherent with the matrix, it is very difficulty for grain or subgrain boundaries to pass by the low energy interfaces between the $Al_3(Sc, Zr)$ particles and the matrix. Therefore, except for Orowan strengthening, grain boundary strengthening provided by $Al_3(Sc, Zr)$ particles can not be ignored, which can be verified by our previous report (Ref 8). Relationship between microstructure and mechanical properties of TIG and FSW joints in the new Al-Mg-Mn-Sc-Zr alloy will be discussed in detail.

The FZ mainly consists of supersaturated solid solution. Therefore, only solution strengthening operates here and the hardness is relatively low. The HAZ suffers lower welding heat than FZ, but its temperature is still higher than 550 °C. $Al_3(Sc,Zr)$ particles partially dissolved in this zone but the rest of particles can still pin the dislocations and sub-boundaries. With the increase of the distance away from the weld center, the substructure strengthening and Orowan strengthening from $Al_3(Sc,Zr)$ particles enhance; hence hardness gradually increases to the level of base metal. As the weld bead in the welded joint can compensate for the strength loss, therefore, the TIG welded joint fails in the HAZ, where the thickness and the strength are lower.

During FSW process, SZ undergoes intense plastic deformation and frictional heating, resulting in the temperature increase up to 400-550 °C (Ref 22, 23). The microstructure of this zone is characterized by fine grains and $Al_3(Sc,Zr)$ particles (Fig. 5). As a result, grain boundary (Hall-Petch or fine grain) strengthening and Orowan strengthening of the nano-scale $Al_3(Sc, Zr)$ particles manifest in this zone, and thus the hardness is relatively high. Due to the experience of high temperature (350-400 °C) (Ref 24, 25) and sever deformation, TMAZ is characterized by deformed grains and lots of dislocation tangles. Consequently, compared with the SZ, grain boundary strengthening is weaker and substructure strengthening enhances. From the TMAZ to the HAZ, due to the decrease of dislocation density, the substructure (dislocation) strengthening decreases, and thus the hardness decreases correspondingly. Hardness levels increase with increasing distance from the HAZ to base metal as substructure hardening becomes more effective. The thickness in the whole weld joint is inhomogeneous and the weld center is the thinnest zone. In addition, compared with base metal, SZ is still a softening zone, and the hardness is only slightly higher than that of the minimum value. Therefore, FSW joints fail in the center of SZ.

4.2 Comparative Analysis of TIG and FSW Joints

From the above experimental results, it can be concluded that for Al-Mg-Mn-Sc-Zr alloy, the FSW joint has better mechanical property than the TIG welded joint. Different performances depend on different microstructures, and different microstructures come from different welding methods. During the TIG welding process, the alloy is melted under high temperature and then solidified, so as-cast structure is formed in the weld joint. What is more, weld defects exist in TIG weld joint, such as gas cavities. These internal welding defects make that the ductility of TIG welded joint is inferior to FSW joint.

For the studied alloy in this paper, the presence of $Al_3(Sc,Zr)$ particles can strongly pin the dislocation and grain boundary, thus effectively restrain recrystallization and remain well preserved cold deformation microstructure. Researchers find that the $Al_3(Sc,Zr)$ particles exhibit good thermal stability; it will not coarsen, keep coherent with Al matrix and can still pin dislocation and grain-boundary even the temperature rise to 500 °C. But when the temperature is up to 550 °C, $Al_3(Sc,Zr)$ particles will coarsen and dissolve and its coherency with matrix will gradually vanish (Ref 26). The alloy in weld center suffered a high temperature of more than 550 °C during the TIG welding process, and the Sc, Zr elements are almost all dissolved in the Al supersaturated solid solution. Therefore, the positive effect of $Al_3(Sc,Zr)$ particles on strength in FZ of TIG welded joint disappears. During FSW, $Al_3(Sc,Zr)$ particles almost keep their nano-scaled size and coherent relationship between matrix in the whole welded joint. Therefore, the precipitation strengthening and grain boundary strengthening from $Al_3(Sc,Zr)$ particles contribute the higher strength in FSW joint.

5. Conclusion

A new Al-5.8%Mg-0.4%Mn-0.25%Sc-0.10%Zr alloy was successfully welded by TIG and FSW techniques. The mechanical properties and microstructure of the welded joints were investigated by microhardness measurements, tensile tests, and microscopy methods. The main results of the current study are as follows:

1. The TIG and FSW joints of the new alloy show high strength and admirable ductility. UTS, YS, elongation to failure are 358, 234 MPa, and 27.6% for TIG welded joint, and 376, 245 MPa, and 31.9% for FSW joint, respectively.
2. The microstructure of Al-Mg-Mn-Sc-Zr alloy is characterized by lots of dislocation tangles and secondary coherent nano-scaled $Al_3(Sc,Zr)$ particles. In TIG welded joint, FZ consists of cast dendritic structure and supersaturated solid solution, and HAZ is made up of deformed elongated grains. For FSW joint, fine-grained microstructure exists in SZ, and thermo-mechanical-affected zone has a highly deformed structure. $Al_3(Sc,Zr)$ particles almost keep their nano-scaled size and coherent relationship between matrix in the whole FSW joint
3. The superior mechanical properties of the TIG and FSW joints of the new alloy are mainly derived from the Orowan strengthening and grain boundary strengthening caused by secondary coherent nano-scaled $Al_3(Sc,Zr)$ nano-particles. For new Al-Mg-Mn-Sc-Zr alloy, the positive effect from secondary $Al_3(Sc, Zr)$ particles can be better preserved in FSW joint than in TIG welded joint.

Reference

1. B. Nie, Z.M. Yin, D.P. Zhu, Y.Y. Peng, F. Jiang, and J.W. Huang, Effect of Homogenization Treatment on Microstructure and Properties of Al-Mg-Mn-Sc-Zr Alloy, *J. Cent. South Univ. Technol.*, 2007, **14**, p 452–455

2. Y. Deng, Z.M. Yin, J.Q. Duan, K. Zhao, B. Tang, and Z.B. He, Evolution of Microstructure and Properties in a New Type 2 mm Al-Zn-Mg-Sc-Zr Alloy Sheet, *J. Alloy. Compd.*, 2012, **517**, p 118–126

3. Yu.A. Filatov, V.I. Yelagin, and V.V. Zakharov, New Al-Mg-Sc Alloys, *Mater. Sci. Eng. A*, 2000, **280**, p 97–101

4. V.G. Davydov, T.D. Rostova, V.V. Zakharov, Yu.A. Filatov, and V.I. Yelagin, Scientific Principles of Making an Alloying Addition of Scandium to Aluminium Alloys, *Mater. Sci. Eng. A*, 2000, **280**, p 30–36

5. Y. Deng, G.F. Xu, Z.M. Yin, X.F. Lei, and J.W. Huang, Effects of Sc and Zr Microalloying Additions on the Recrystallization Texture and Mechanism of Al-Zn-Mg Alloys, *J. Alloy. Compd.*, 2013, **580**, p 412–426

6. Y. Deng, B. Peng, G.F. Xu, Q.L. Pan, Z.M. Yin, R. Ye, Y.J. Wang, and L.Y. Lu, Effects of Sc and Zr on Mechanical Property and Microstructure of Tungsten Inert Gas and Friction Stir Welded Aerospace High Strength Al-Zn-Mg Alloys, *Mater. Sci. Eng.*, 2015, **639**, p 500–513

7. Y. Deng, Z.M. Yin, K. Zhao, J.Q. Duan, and Z.B. He, Effects of Sc and Zr Microalloying Additions on the Microstructure and Mechanical Properties of New Al-Zn-Mg Alloys, *J. Alloy. Compd.*, 2012, **530**, p 71–80

8. Y. Deng, B. Peng, G.F. Xu, Q.L. Pan, Z.M. Yin, R. Ye, Y.J. Wang, and L.Y. Lu, Effects of Sc and Zr on Mechanical Property and Microstructure of Tungsten Inert Gas and Friction Stir Welded Aerospace High Strength Al-Zn-Mg Alloys, *Mater. Sci. Eng. A*, 2015, **639**, p 500–513

9. J.S. Vetrano, S.M. Bruemmer, L.M. Pawlowski, and I.M. Robertson, Influence of the Particle Size on Recrystallization and Grain Growth in Al-Mg-X Alloys, *Mater. Sci. and Eng. A*, 1997, **238**, p 101–107

10. X.F. Lei, Y. Deng, Z.M. Yin, and G.F. Xu, Tungsten Inert Gas and Friction Stir Welding Characteristics of 4-mm-Thick 2219-T87 Plates at Room Temperature and −196 °C, *J. Mater. Eng. Perform.*, 2014, **23**, p 2149–2158

11. Z.B. He, Y.Y. Peng, Z.M. Yin, and X.F. Lei, Comparison of FSW and TIG Welded Joints in Al-Mg-Mn-Sc-Zr Alloy Plates, *Trans. Nonferrous Met. Soc. China*, 2011, **21**, p 1685–1691

12. Y. Deng, R. Ye, and G.F. Xu, Corrosion Behaviour and Mechanism of New Aerospace Al-Zn-Mg Alloy Friction Stir Welded Joints and the Effects of Secondary $Al_3Sc_xZr_{1-x}$ Nanoparticles, *Corros. Sci.*, 2015, **90**, p 359–374

13. A. Squillace, A. De Fenzo, G. Giorleo, and F. Bellucci, A Comparison between FSW and TIG Welding Techniques: Modifications of Microstructure and Pitting Corrosion Resistance in AA 2024-T3 Butt Joints, *Mater. Process. Technol.*, 2004, **152**, p 97–105

14. E. Taban and E. Kaluc, Comparison Between Microstructure Characteristics and Joint Performance of 5086-H32 Aluminium Alloy Welded by MIG, TIG and Friction Stir Welding Processes, *Kovove Mater.*, 2007, **45**, p 241–248

15. J.Q. Su, T.W. Nelson, R. Mishra, and M. Mahoney, Microstructural Investigation of Friction Stir Welded 7050-T651 Aluminium, *Acta Mater.*, 2003, **51**, p 713–729

16. M. Ericsson and R. Sandstrom, Influence of Welding Speed on the Fatigue of Friction Stir Welds, and Comparison with MIG and TIG, *Int. J. Fatigue.*, 2003, **25**, p 1379–1387

17. J. Zhao, F. Jiang, H.G. Jian, K. Wen, L. Jiang, and X.B. Chen, Comparative Investigation of Tungsten Inert Gas and Friction Stir Welding Characteristics of Al-Mg-Sc Alloy Plates, *Mater. Des.*, 2010, **31**, p 306–311

18. S. Lathabai and P.G. Lloyd, The Effect of Scandium on the Microstructure, Mechanical Properties and Weldability of a Cast Al-Mg Alloy, *Acta Mater.*, 2002, **50**, p 4275–4292

19. Y.Y. Peng, Z.M. Yin, X.F. Lei, Q.L. Pan, and Z.B. He, Microstructure and Properties of Friction Stir Welded Joints of Al-Mg-Sc Alloy Plates, *Rare Metal Mater. Eng.*, 2011, **40**(2), p 0201–0205

20. Y. Deng, B. Peng, G.F. Xu, Q.L. Pan, R. Ye, Y.J. Wang, L.Y. Lu, and Z.M. Yin, Stress Corrosion Cracking of a High-Strength Friction-Stir-Welded Joint of an Al-Zn-Mg-Zr Alloy Containing 0.25 wt.% Sc, *Corros. Sci.*, 2015, **90**, p 359–374

21. P.M.G.P. Moreira, M.A.V. de Figueiredo, and P.M.S.T. de Castro, Fatigue Behaviour of FSW and MIG Weldments for Two Aluminium Alloys, *Theor. Appl. Fracture Mech.*, 2007, **48**, p 169–177

22. Z.L. Hu, X.S. Wang, and S.J. Yuan, Quantitative Investigation of the Tensile Plastic Deformation Characteristic and Microstructure for Friction Stir Welded 2024 Aluminum Alloy, *Mater. Charact.*, 2012, **73**, p 114–123

23. B. Heinz and B. Skrotzki, Characterization of a Friction-Stir-Welded Aluminum Alloy 6013, *Metall. Mater. Trans. B*, 2002, **33**, p 489–498

24. M. Chemingui, M. Khitouni, K. Jozwiak, G. Mesmacque, and A. Kolsi, Characterization of the Mechanical Properties Changes in an Al-Zn-Mg Alloy After a Two-Step Ageing Treatment at 70 and 135 °C, *Mater. Des.*, 2010, **31**, p 3134–3139

25. Y.M. Hwang, Z.W. Kang, Y.C. Chiou, and H.H. Hsu, Experimental Study on Temperature Distributions Within the Workpiece During Friction Stir Welding of Aluminum Alloys, *Int. J. Machine Tools Manuf.*, 2008, **48**, p 778–787

26. P. Cavaliere and M. Cabibbo, Effect of Sc and Zr Additions on the Microstructure and Fatigue Properties of AA6106 Produced by Equal-Channel-Angular-Pressing, *Mater. Charact.*, 2008, **59**, p 197–203